

Dissolution of Selected Trace Elements from Simulated Atmospheric Aerosol Aging and Human Exposure of Mineral Dust and Coal Fly Ash

Nausheen W. Sadiq,* Catharina Venter, Wisam Mohammed, Yara Khalaf, and Hind A. Al-Abadleh*



Cite This: *ACS EST Air* 2024, 1, 5–15



Read Online

ACCESS |

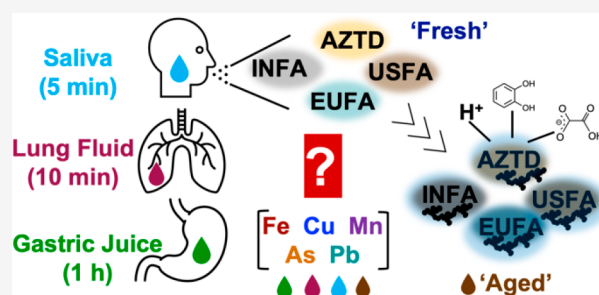
Metrics & More

Article Recommendations

Supporting Information

ABSTRACT: Atmospheric particles from natural and anthropogenic sources contain reactive trace elements (TE) of importance to aerosol multiphase chemistry, health risk assessment of inhalation and ingestion, and ocean productivity. While the dissolution of TE from model and field-collected particles in various aqueous phase conditions of relevance to aerosol liquid water and bodily fluids have received attention, there remain knowledge gaps on (a) benchmark materials and methods for standardizing dissolution experiments and (b) the relevance of dissolution time scales in previously published reports to real-time, long range transport and human exposure. Here, we use fully characterized reference solid materials, namely, Arizona test dust (AZTD) and combustion coal fly ash samples from India, the U.S., and Europe, representative of atmospheric aerosol particles from natural and combustion sources. Using ICP-MS and optimized analytical procedures that address technical challenges with selectivity and sensitivity, we quantified the concentrations of dissolved TE Fe, Cu, Mn, As, and Pb under simulated atmospheric aging (14 days) and human exposure experiments using saliva (5 min), lung fluid (10 min), and gastric juice (1 h). We found that levels of dissolved TE normalized to the total dissolvable levels under strong acid extraction are much higher in simulated aged aerosol water than in bodily fluids of unreacted particles. The significance of these results is discussed in the context of aerosol multiphase chemistry, health impacts, and ocean biogeochemistry.

KEYWORDS: *Arizona test dust, fly ash, trace elements, brown carbon, aerosol aging, bioaccessibility, health risk assessment, ocean productivity*



INTRODUCTION

The trace elements (TE), which include transition metals and metalloids, in atmospheric aerosol particles originate from natural and anthropogenic sources. Wind action on the Earth's crust produces mineral dust aerosol during major storm events resulting in thousands of teragrams in atmospheric loading.^{1,2} These aerosols cover the coarse and super-coarse size modes (diameter (d) > 1 μm) with a smaller fraction in the higher surface area accumulation mode ($0.1 < d < 1 \mu\text{m}$). These particles undergo long range transport for thousands of kilometers.^{3–6} Aerosol particles in the latter size range are more reactive and have longer atmospheric residence time.^{7–9} The burning of fossil fuels and waste, traffic and industrial activities also produce “unconventional” mineral dust called coal fly ash and oil fly ash, mostly in the fine ($d < 2.5 \mu\text{m}$) and ultrafine size modes ($d < 0.1 \mu\text{m}$).^{10,11} TE in natural and unconventional mineral dust appear in the form of oxides, carbonates, and sulfates in a matrix of clays and oxides of alkali and alkaline earth metals.^{12–16} These elements include Fe, Cu, Mn, As, and Pb, which are the focus of our studies here. A broad classification of these elements on a global scale list as traffic-related (Fe and Mn),¹⁷ traffic/industrial (Cu),¹⁷ and

industrial/burning (As and Pb).¹⁸ The relative amounts of these elements vary by location and level of traffic/industrial activities.

Atmospheric aerosol particles containing TE have complex physicochemical properties that evolve over time due to atmospheric aging, a term referring to multiphase reactions with reactive radicals, acidic gases, and organics.¹⁹ Out- and in-cloud processing of these particles also take place due to changes in relative humidity, temperature, and pH.^{20–22} Some of these reactions and processes are catalyzed by transition metals in mineral dust and fly ash and enhance TE dissolution, particularly in the presence of water soluble organic carbon (WSOC).^{23,24} For example, the speciation, chemistry and dissolution of Fe in mineral dust and fly ash particles received

Received: July 6, 2023

Accepted: September 5, 2023

Published: November 29, 2023



Table 1. Characterization of Sample Particles Used in Experiments

sample	specific BET surface area (m ² g ⁻¹)	most probable size/diameter (μm) and shape	minerals identified from XRD data	ref
AZTD	26 ± 1	2 ± 1 rock-like (assume cube)	muscovite (33.4%), quartz (30.7%), albite (10.9%), kaolinite (9.1%), sanidine (7.8%), and calcite (5.4%)	54
		0.6 ± 0.3 rock-like	muscovite (H ₂ KAl ₃ Si ₃ O ₁₂), quartz (SiO ₂), albite (Na _{0.98} Ca _{0.02} Al _{1.02} Si _{2.98} O ₈), calcite (CaCO ₃), kaolinite (H ₄ Al ₂ Si ₂ O ₉), paulmooreite (Pb ₂ As ₂ O ₅), lead manganate (Pb(MnO ₄)), copper iron oxide (CuFe ₂ O ₄)	this work
INFA	0.98 ± 0.03	1.21 ± 0.06 spherical	mullite	53
		1.3 ± 0.3	mullite (Al _{2.32} Si _{0.68} O _{4.48}), quartz (SiO ₂), iron oxide (Fe _{2.811} O ₄)	this work
USFA	1.8 ± 0.1	0.89 ± 0.08 spherical	mullite	52,53
		0.9 ± 0.4 spherical	halite (NaCl), anhydrite (Ca(SO ₄)), sylvite, syn (KCl), calcite, syn (CaCO ₃), graphite-2H (C), gismondine (CaAl ₂ Si ₂ O _{8.4} H ₂ O)	this work
EUFA	2.8 ± 0.1	2.2 ± 0.2 rock-like (assume cube)	mullite, calcium feldspars, calcite	52,53
		0.2 ± 0.1 rock-like	halite, syn (NaCl), anhydrite (Ca(SO ₄)), sylvite, syn (KCl), calcite, syn (CaCO ₃), graphite-2H (C), vaterite, syn (CaCO ₃), cuprite (CuO), bixbyte (MnFeO ₃), calcium aluminum oxide (Ca ₃ Al ₂ O ₆)	this work

much attention because Fe is a redox (photo)active element and an essential micronutrient for organisms at the sea surface microlayer.^{20,25,26} Multiphase chemistry in atmospheric aerosols changes the aerosol hygroscopicity²⁷ and acidity,²⁸ surface and bulk chemical composition,²⁹ optical properties,³⁰ morphology,³¹ and mixing state.³² These changes control the aerosol residence time in the atmosphere and impact the climate system. Also, the insoluble and dissolved transition metal content in aerosol liquid water determine the biological and toxicological impacts of atmospheric aerosols.^{33–37} Studying these impacts is of importance to understanding and quantifying aerosol effects on ocean productivity upon deposition and human health upon inhalation-ingestion.

Numerous studies highlight the impacts of inhaling particulate matter (PM) in the fine (<2.5 μm, referred to as PM_{2.5}) and ultrafine (<0.1 μm, PM_{0.1}) size range on human health and their links to cardiovascular diseases, lung cancer, brain function damage, and mortality.^{38,39} Park et al.⁴⁰ analyzed the differential toxicity of PM_{2.5} from various combustion and noncombustion sources to derive toxicity scores. Traffic-related PM_{2.5} from road dust, break and tire wear⁴¹ yielded the highest toxicity scores. Chemical toxicity studies assess the bioaccessibility of metals in PM by using assays to quantify the fraction of soluble metal in bodily fluids to accurately estimate the PM oxidative potential^{33,42–45} following inhalation-ingestion.^{46,47}

The working definition of “bioaccessibility” is “the fraction of a compound that is released from its matrix [to the surrounding such as] the gastrointestinal tract, and thus becomes available for intestinal absorption (i.e., enters the bloodstream)”⁴⁸ or for uptake by biota at the sea surface microlayer (SML).^{35,49} This term includes all the mechanistic steps that take place post inhalation-digestion and deposition on the SML that essentially dissolve TE from PM. The final speciation of these TE in the surrounding depends on the pH, type, and concentration of WSOC.⁵⁰ The term “bioavailability” is “the sum of bioaccessibility and bioactivity, which refers to the transport and biochemical processes within tissues”.⁴⁸ This term is also applicable for similar processes in microorganisms.³⁶ Quantifying fully bioaccessible metals from airborne PM is the first step for modeling the pool of dissolved metals for health risk assessment and biogeochemical processes in the SML,³⁶ respectively. For example, on the former, Schaffler et al.⁵¹ measured the total concentrations and leaching of several potentially toxic elements that include Cu,

As, and Pb from PM collected on filters with simulated saliva, gastric juice, and lung fluid. They found that 2.5% of Cu and As are released in saliva (10 min, pH 6.5) compared to 26% in gastric juice (2 h, pH <1). The highest release of Pb (77% and 61%) was in gastric juice (2 h) and lung fluid (56 h, pH 7.4), respectively. These results highlight the dependency of the concentrations on the chemical composition and pH of the fluids in which the dissolution of PM is taking place in relation to assessing health risks.

A critical look at the above studies revealed three major gaps in knowledge: (1) the effect of atmospheric aging processes over times that simulate long range transport (14 days, abbreviated to 14-d onward) on the dissolution of TE from natural and combustion sources, (2) the dissolution of TE from natural and combustion sources in bodily fluids (saliva, lung, and gastric) over times that simulate human exposure (10 min to 1 h), and (3) lack of results from using readily available and fully characterized reference solid materials, which are representative of atmospheric aerosol particles from natural and combustion sources, using state of the art analytical methods that address technical challenges with selectivity and sensitivity. Our studies here aim to address these gaps of knowledge using commercially available Arizona test dust (AZTD) and combustion coal fly ash samples from India, the U.S. and Europe previously characterized and studied for Fe solubility under various atmospherically-relevant conditions.^{52,53} While AZTD does have differences with ambient dust samples collected in the atmosphere, it is used here as a standard benchmark so that composition and reactivity of field particles collected by different research groups could be compared to it. Simulated atmospheric aging and human exposure experiments were conducted to quantify the dissolution of TE from the above solids. By varying the bodily fluid exposure time, optimizing the lung fluid utilized, applying a microwave extraction method vs a simplified hot block digestion, and incorporating the high matrix introduction (HMI) mode on the Agilent 7850, our studies here allow for enhanced extraction and analysis than what has been used in past studies. The HMI mode allows samples to be analyzed without a need for a high dilution and thus produces more precise results. The data below clearly show that atmospheric aging of mineral dust and fly ash particles over 14-d under acidic conditions is more efficient than bodily fluids in dissolving essential micronutrient and potentially toxic TE. As detailed in the implications section, these studies suggest

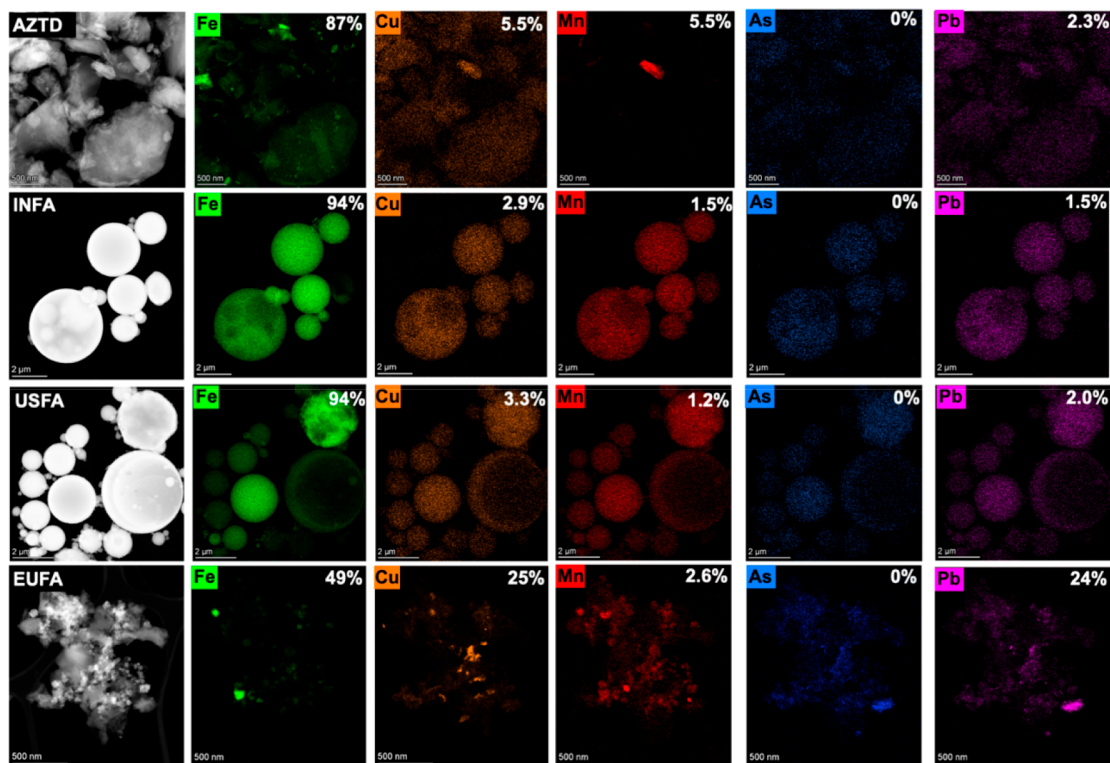


Figure 1. Scanning transmission electron microscopy (STEM) images of the solids used in our studies with elemental mapping. The percentages listed are % mass fraction are from the quantification of the elements in the energy dispersive X-ray spectroscopy (EDS) maps, where the software was carefully calibrated with standard samples.

that inhaling-ingestion and deposition of aged atmospheric particles would influence ocean biogeochemistry and pose a larger health risk than freshly emitted ones.

MATERIALS AND METHODS

Chemicals. All chemicals were used as received without further purification. Table 1 lists the solids received from Prof. Juan Navea, who characterized these particles for specific Brunauer–Emmett–Teller (BET) surface area using N_2 gas as an adsorbent, most probable size and shape, and mineralogy in earlier publications.^{52–54} In our studies, electron microscopy images, elemental mapping spectra, and micro X-ray diffraction spectra were collected at the Canadian Centre for Electron Microscopy and the MAX Diffraction Facility located at McMaster University for size, shape, spatial distribution, and crystalline phases of the elements studied here. More details on the solids characterization, sources, purity, physical properties of the organics, and description of solution preparation are provided in the Supporting Information (SI) and Table S1.

Simulated Atmospheric Aging Experiments. Sixty samples (divided into five sets) were prepared using four different mediums; one set contained 1 g L^{-1} AZTD, three sets were composed of 1 g L^{-1} fly ash slurry (INFA, USFA, or EUFA), and one control set containing Milli-Q water ($18.2\text{ M}\Omega\text{-cm}$). Comparisons between the absence of organics versus the presence of catechol or oxalic acid were observed over the course of a 14-d dark reaction simulation. These organics were chosen as the simplest proxies for reactive phenolic compounds and dicarboxylic acids commonly detected in WSOC. Both organics promote surface-catalyzed reactions, including abiotic oxidative polymerization and dissolution of TE, respectively. The final concentration of each organic was 1

mM. Detailed calculations on the atmospheric relevance of this concentration for deliquesced aerosols are provided in the SI. Diluted hydrochloric acid (HCl, 6 M, Ricca Chemical Company) was used to obtain the desired pH ranging from pH 1–9. This pH range is atmospherically relevant because it covers aerosol pH for highly acidic and processed aerosol liquid water, near neutral cloud/fog water, and basic adsorbed water on freshly emitted mineral dust particles.^{19,28} The pH of the slurries was measured as a function of time over the 14-d period. At the end of the experiment on day 14, the slurries were filtered using $0.2\text{ }\mu\text{m}$ nylon filters and the filtrates were analyzed using ICP-MS for the level of TE. Additional details are provided in Figure S1 and the SI.

Simulated Human Exposure Experiments. Three different simulated lung fluids were tested with AZTD in order to optimize results: the Beauchemin lab fluid,⁵¹ Gamble fluid,⁵⁵ and an in-house modified Hatch fluid. Subsequent bioaccessibility experiments were conducted on USFA and INFA, in which samples were subjected to timed trials, and supernatants were collected after centrifugation. Separate experiments were conducted on all samples with varying exposure times to artificial saliva and gastric juice.⁵⁶ Microwave digestion was used to treat any remaining residue in all experiments. More details are provided in Table S2, Figures S2–S4, and the SI.

Elemental Analysis Using ICP-MS. To determine the maximum TE content in the solids listed in Table 1, samples were analyzed at ALS Global using ICP-MS per EPA method 6020B (mod)⁵⁷ following sample preparation with strong acid (HNO_3/HCl) extraction according to EPA method 200.2 (mod).⁵⁸ For the simulated atmospheric aging and human exposure experiments, the dissolved metal content was

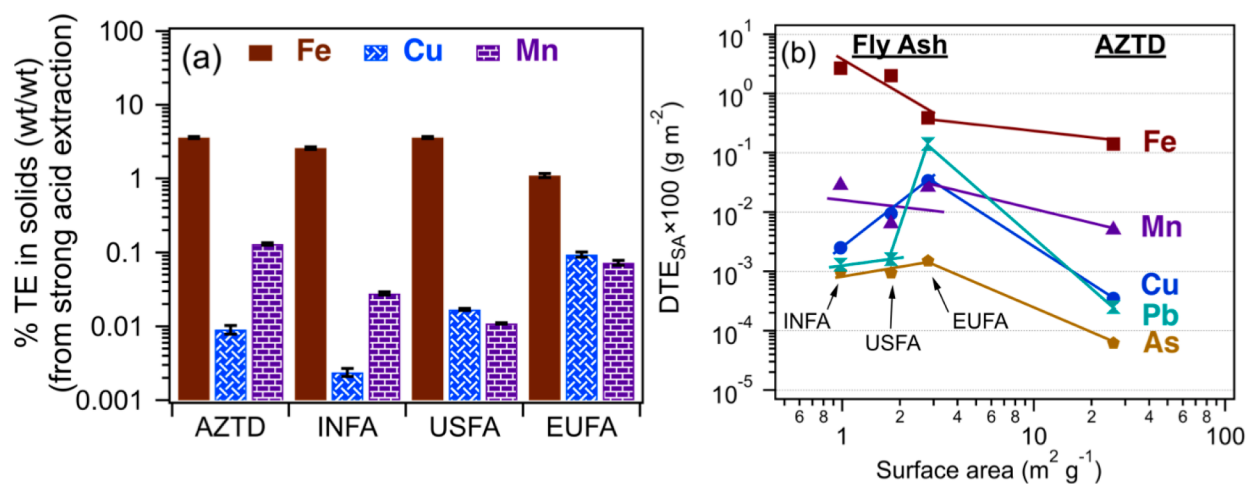


Figure 2. Amount of dissolved transition metals Fe, Cu, and Mn solubilized from the strong acid extraction per EPA method 6020B (mod) expressed as (a) percentage relative to the total solid mass of the respective material according to eq 1 and (b) normalized to the BET surface area of the respective material according to eq 2. The raw data are listed in Table S4.

determined using an Agilent 7850 ICP-MS instrument equipped with High Matrix Introduction (HMI) mode and a Helium collision cell for all metals analysis. Samples were diluted and filtered prior to analysis using 0.45 μm poly-(tetrafluoroethylene) (PTFE) syringe filters. Matrix-matched external calibration was utilized, and a multielemental calibration curve was created spanning from 0.1 ppb to 1 ppm for all metals studied (Inorganic Ventures). More details are provided in Table S3 and the SI.

RESULTS AND DISCUSSION

1. Trace Element Distribution in the Solids and Dissolvable Amounts from Strong Acid Extraction Methods. Elemental maps of the solids used here in relation to particles' sizes and shapes are shown in Figure 1. The particle shape, which is described in Table 1, agrees with those of previous studies. The trend in the size distribution of the fly ash samples agrees better with the trend in surface area values, where the smallest size distribution of $0.2 \pm 0.1 \mu\text{m}$ for EUFA resulted in $2.8 \pm 0.1 \text{ m}^2 \text{ g}^{-1}$ compared to the larger size distribution of $1.3 \pm 0.3 \mu\text{m}$ for INFA with $0.98 \pm 0.03 \text{ m}^2 \text{ g}^{-1}$. Results from micro-XRD measurements are also listed in Table 1. We specifically looked for solid phases containing the elements in this study. For AZTD, paulmooreite ($\text{Pb}_2\text{As}_2\text{O}_5$), lead manganate ($\text{Pb}(\text{MnO}_4)$), and copper iron oxide (CuFe_2O_4) were identified as potential phases in addition to the clays identified in previous studies. The XRD spectrum for INFA showed the potential presence of iron oxide ($\text{Fe}_{2.811}\text{O}_4$). There were no additional peaks left to match with additional phases to account for the presence of Cu, Mn, As, and Pb. The USFA and EUFA spectra showed the potential presence of phases containing Na, K, Cl, Ca, S and graphite, which were not reported earlier. The spectrum for EUFA had peaks that matched cuprite (CuO) and bixbyite (MnFeO_3).

The distribution of Fe, Cu, Mn, and Pb in the AZTD and EUFA particles appears less uniform compared to INFA and USFA. The signal from As is too low relative to the background due to trace amounts. The images also showed no collocation of Fe with either Cu or Mn in AZTD, and some collocation between Fe and Mn, and between As and Pb for EUFA. All of the elements shown in Figure 1 appear collocated in the INFA and USFA particles, especially the largest size

ones for the latter. The percentage mass fraction for each element in Figure 1 shows that Fe is the major TE in AZTD, INFA, and USFA (greater than 85%), followed by Cu and Mn with similar levels between 1 and 6%, then Pb between 1 and 2.5%. Fe mass fraction in EUFA is lower than the other solid at 49% followed by Cu and Pb at 25 and 24%, respectively, then Mn at 2.6%. These elemental mass fractions in the solids are useful for comparison with the values obtained from strong acid extraction.

Figure 2a shows selected weight percentages of the top three dissolved TE (DTE) by mass in AZTD, INFA, USFA, and EUFA, namely, Fe, Cu, and Mn following extraction in strong acids such as HNO_3 and HCl used in the determination of total trace metal content in solids by ICP-MS per EPA method 6020B (mod).⁵⁷ This experimental procedure aims to solubilize most of the metals in the solid matrix. These percentages were calculated according to eq 1:

$$\% \text{DTE} = \frac{[\text{TE}(\text{aq})]_{\text{acid_extr}} (\mu\text{g g}^{-1})}{10^6 \mu\text{g g}^{-1}} \cdot 100 \quad (1)$$

The mass-normalized data in Figure 2a show that Fe levels are about 1–2 orders of magnitude higher than those of Cu and Mn depending on the solid. The levels of Mn are higher by 1 order of magnitude than Cu in AZTD and INFA, whereas the levels of both elements are similar for USFA and EUFA. Similar data for As and Pb are shown in Figure S5, where both elements are below 0.01% (w/w) for AZTD, INFA, and USFA. In the case of EUFA, Pb and As levels are about 0.4% and 0.005% (w/w), two- and five-orders of magnitude higher than other solids.

The dissolved amounts of the TE normalized to the BET surface area (DTE_{SA}) is shown in Figure 2b. These amounts were calculated according to eq 2:

$$\text{DTE}_{\text{SA}} (\text{g m}^{-2}) = \frac{[\text{TE}(\text{aq})] (\mu\text{g g}^{-1})}{\text{specific BET area of particles} (\text{m}^2 \text{ g}^{-1}) \cdot 10^6 \mu\text{g g}^{-1}} \cdot 100 \quad (2)$$

For each solid, the values of DTE_{SA} show that the Fe content is 1–2 orders of magnitude higher than Cu and Mn, followed by Pb and As. Similar trends were also obtained when the % mass fraction of each TE in Figure 1 was normalized to the BET surface area. The normalization of the trace element content to

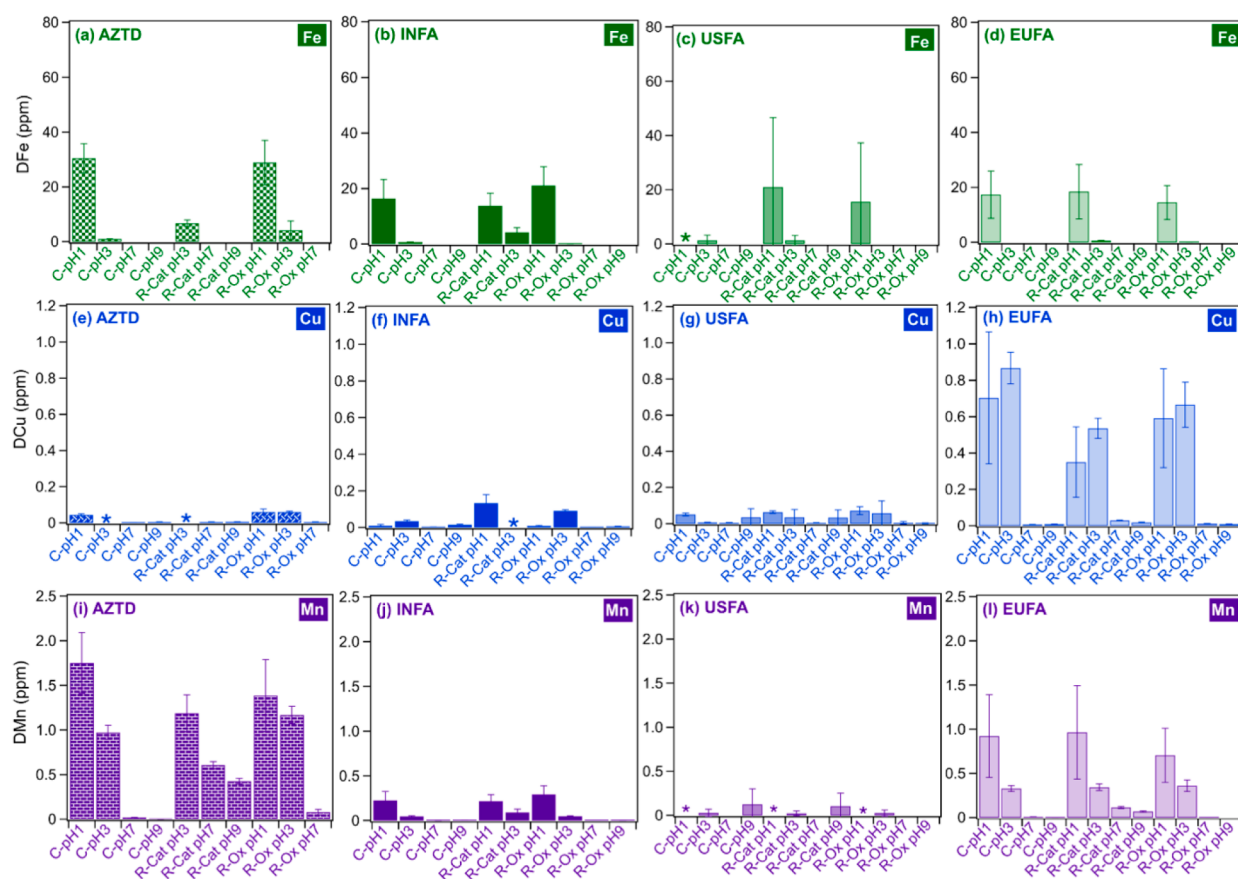


Figure 3. Concentration of dissolved Fe (top), Cu (middle), and Mn (bottom) in ppm (mg L^{-1}) after a 14-d simulated atmospheric aging experiment of each respective material as a function of pH, in the absence and presence of soluble organic catechol (Cat) and oxalic acid/oxalate (Ox). The “*” denotes omission of data due to instrumental issues that affected the raw data. Grids with no data indicate that numbers were below the detection limit.

surface area shows that AZTD, with the highest measured BET surface area, did not produce the highest dissolvable amounts of the TE compared to the fly ash samples. This result emphasizes that the rate of dissolution in the strong acid extraction procedure is affected to a higher degree by the mineralogy, morphology, and density of defects than surface area only, as shown in a number of studies for Fe.^{16,59,60} Within the fly ash samples, there are negative linear trends for DTE_{SA} with increasing surface area for Fe and Mn, and positive linear trends for Cu, Pb, and As. These results clearly show the differences in the dissolution mechanisms of metal oxides in fly ash samples despite the same experimental conditions, which needs further investigation to disentangle the role of surface area from the roles of mineralogy and surface defects.⁶¹ The following section describes results from simulated dark atmospheric aging experiments as a function of pH without and with catechol and oxalic acid as proxies for reactive WSOC.

2. Soluble Trace Metal Content from Simulated Atmospheric Aerosol Aging Experiments. As stated in the introduction, dark processing of mineral dust and fly ash particles takes place in the atmosphere due to the uptake of acidic gases such as hydrochloric and nitric acids, reactive dicarboxylic acids, and phenolic compounds. These organic compounds are commonly detected in WSOC and result in promoting surface-catalyzed reactions, including dissolution of TE. Figures S6 and S7 show digital images of the control and

reaction vials at starting pH 1 and 7 for days 0 and 14 along with the final pH. These images show qualitative changes in the color of the slurries relative to the control vial in the absence of the particles. One of the main two observations from these figures is that reaction vials containing catechol are relatively darker in color on day 14 compared to those with no organics and those with oxalic acid. The most dramatic change observed for USFA was for samples starting at pH 1 and all slurries starting at pH 7. This darkening in color was observed previously for AZTD due to the Fe-catalyzed oxidative polymerization of catechol that leads to the formation of polycatechol.⁵⁴ Due to the presence of Fe in the fly ash samples used here at levels comparable to those in AZTD, similar surface chemistry is taking place with catechol. In the control vial with no dust or fly ash particles, catechol undergoes auto-oxidation in the presence of dissolved oxygen at a much slower rate than in the presence of Fe.^{62,63}

The second main observation from the images in Figures S6 and S7 is the change in the measured bulk pH for the control and slurry vials on day 14 of the simulated atmospheric aging experiments. Figure S8 tracks the pH change as a function of time during the 14-d period. While the pH values changed by ± 0.1 – 0.3 for the starting pH 1, as shown in Figures S6 and S7, the pH change was much higher, ranging from 3 to 10.6 for the starting pH 7, depending on the sample. The slurries of USFA and EUFA with no organics resulted in higher pH values by two to three units on day 14, from 7 to 10.6 and 8.6,

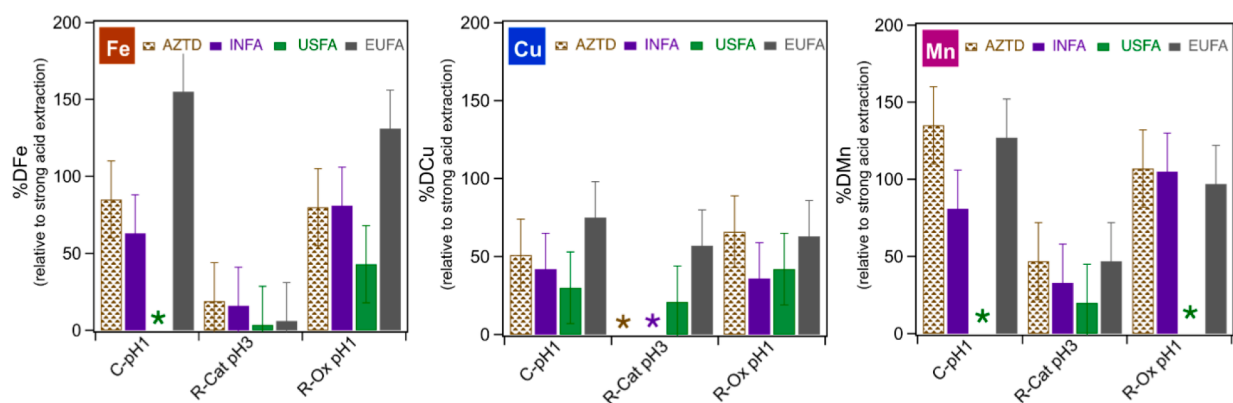


Figure 4. Amount of dissolved transition metals Fe, Cu, and Mn after 14-d simulated atmospheric aging experiments, expressed as a percentage relative to the respective dissolved metals from the strong acid extraction of each respective material according to eq 3. The “*” denotes omission of data due to instrumental issues that affected raw values.

respectively. This is due to the higher percentages of basic metal oxides such as CaO and MgO in these fly ash samples compared to those of AZTD and INFA. Table S5 lists the percentages of Ca and Mg to Al from the strong acid extraction and atmospheric aging experiments at pH 1 and 7. There are statistically significant higher amounts of Ca and Mg in the USFA and EUFA compared to AZTD and INFA by factors ranging from 2 to 6 under acidic and neutral experimental conditions. This observation underscores the importance of studying surface reactions of atmospheric relevance under basic bulk pH. The pH of the reaction slurry vials containing catechol was lower by two units relative to that of the control slurries with no catechol. This is because the aqueous phase^{62,63} and surface-catalyzed oxidative polymerization of catechol⁵⁴ releases protons to the solution that lower the bulk pH. For the reaction vials containing oxalic acid, the pH change was between 1 and 2 units higher than the starting pH, likely due to ligand exchange with surface hydroxyl groups during the inner-sphere complexation of oxalate.

In addition, Figures 3 and S9 show the concentrations of dissolved Fe, Cu, Mn, As, and Pb at the end of the simulated dark atmospheric aging experiments of AZTD, INFA, USFA, and EUFA as a function of pH in the absence and presence of organics. There is a clear nonlinear pH dependence on the level of the TE, with the highest dissolved amounts at pH 1 and then pH 3 for Fe, Mn, As, and Pb. The trend is reversed for Cu, where the highest dissolved amounts were observed at pH 3 then at pH 1. The concentration values shown in Figures 3 and S9 were converted to percentages of dissolved TE relative to the dissolvable fraction using strong acid extraction according to eq 3:

$$\%DTE = \frac{[TE(aq)] \text{ (mg L}^{-1}\text{)} \cdot \text{vol of slurry (L)}}{\text{amt of particles in slurry (g)} \cdot [TE(aq)]_{\text{acid_extr}} \text{ (}\mu\text{g g}^{-1}\text{)}} \cdot 100 \quad (3)$$

Figures 4 and S10 show the variability in %DTE for selected acidic conditions, control (no organics), and reacted with catechol and oxalic acid for the dust and fly ash samples studied here. Identical results were obtained when multiplying the numerator and denominator by the specific BET surface area of each solid. Hence, the calculation of %DTE accounts for the surface area effects. Within the uncertainty of the measurements, the %DFe levels in Figure 4 are highest for EUFA at pH 1 without and with oxalic acid. For AZTD, the %DFe levels are statistically similar. In the case of INFA, the average data in

Figure 3b show that DFe is about 21 ± 7 ppm for R-Ox pH 1 compared to 16 ± 7 ppm for C-pH 1, which is equivalent to a %DFe of 81 ± 20 and $63 \pm 16\%$, respectively. This result highlights the role of oxalate in promoting iron oxide dissolution under acidic conditions. Data for USFA at pH 1 are shown only with catechol and oxalic acid because analysis of control samples with no organics was irreproducible due to instrumental issues.

At pH 1, the speciation of aqueous oxalic acid is 50% $H_2C_2O_4$ and 50% $HC_2O_4^-$, whereas at pH 3, it is about 85% $HC_2O_4^-$ and 10% $C_2O_4^{2-}$.⁶⁴ The increase in the concentration of singly and doubly deprotonated oxalate species increases the importance of ligand-promoted dissolution relative to that of the control with no oxalic acid. For example, the data in Figure 3a for AZTD show that DFe is about 4 ± 3 ppm for R-Ox pH 3 compared to 1 ppm for C-pH3, which is equivalent to %DFe of 12 ± 3 and 3%, respectively. These results highlighting oxalate-promoted dissolution of iron oxides are similar to those reported by Paris and Desboeufs⁶⁵ for Niger dust at pH 4.7 after 60 min, and Chen and Grassian⁵⁹ for AZTD at pH 2 as a function of time up to 45 h. The %DFe values for AZTD and INFA are statistically lower than EUFA at pH 1 with no organics. All fly ash samples showed a major reduction in %DFe at pH 3 compared to pH 1 under our experimental conditions without and with organics, which made it hard to discern the role of oxalate relative to the control. While Chen and Grassian⁵⁹ reported dark oxalate-promoted dissolution of iron oxides in fly ash samples at pH 2 over 45 h, several experimental differences contribute to the apparent discrepancy between our results here and theirs. These differences include pH (1 and 3 compared to 2), solid loading (1 g L^{-1} compared to 2 g L^{-1}), and oxalate concentration (1 mM compared to 11.7 mM). The relatively higher fly ash loading and oxalate concentration would nonlinearly increase the dissolution rate and hence amplify the role of oxalate under acidic conditions. The presence of catechol drastically reduced %DFe at pH 3 for all of the solids studied, with AZTD and INFA showing higher average %DFe (and hence reactivity) than the rest of the solids.

For %DCu, the acidic conditions of the simulated atmospheric aging resulted in about 50-75% average relative to the dissolvable fraction using strong acid extraction. Within the uncertainty of the measurements, AZTD and EUFA showed the highest values of %DCu followed by USFA and INFA. The data do not show an effect for catechol and oxalic

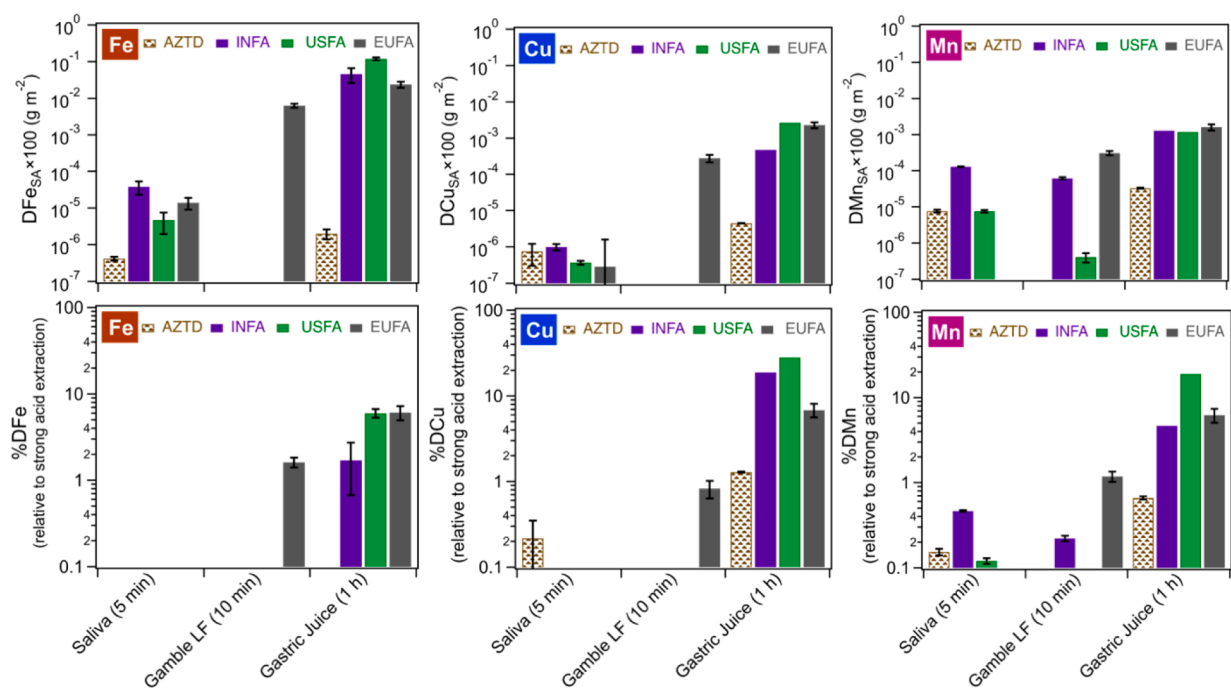


Figure 5. Amount of dissolved transition metals Fe, Cu, and Mn after extraction experiments in bodily fluids specified along the x-axis: (upper) after normalization to the BET surface of each respective material according to eq 2, and (lower) relative to the respective dissolved metal from the strong acid extraction listed in Table S4 according to eq 4.

acid at pH 1 on the %DCu values. On the other hand, the acidic conditions of the simulated atmospheric aging without and with oxalic acid at pH 1 resulted in %DMn near 100% for the dust and fly ash samples studied here, except USFA for which data are not available. Within the uncertainty of the measurements, the presence of catechol resulted in lower %DMn at pH 3. These results show that for the top three transition metals in dust and fly ash samples, most of the dissolvable fraction of Fe and Mn becomes part of highly acidic atmospheric aerosol water without and with oxalic acid compared with nearly half of the dissolvable Cu. Also, catechol appears to lower the levels of dissolved Fe in acidic atmospheric aerosol water to a higher degree than that of Mn and Cu.

Furthermore, Figure S10 shows selected %DAs and %DPb at the end of the 14-d simulated atmospheric aging experiment under acidic conditions without and with organics. Within the uncertainty of the measurements, these experimental conditions resulted in releasing nearly 100% of dissolvable As from INFA and EUFA samples, compared to nearly 50% from AZTD and USFA samples at pH 1 without and with oxalic acid. The presence of catechol at pH 3 resulted in statistically lower %DAs compared to oxalic acid and no organics, with INFA releasing nearly 50% of the dissolvable As. In the case of %DPb, the data in Figure S10 show that for AZTD at pH 1 with no organics, an average of 60–70% of dissolvable Pb is present in the aqueous phase compared to nearly 100% in the presence of catechol and about 25% in the presence of oxalic acid. While EUFA has the highest Pb content on a per mass basis as shown in Figure S5, nearly 70% of that amount is dissolvable under simulated atmospheric aging conditions. Data for USFA show statistically lower %DPb with EUFA at pH 3 with catechol and oxalate. A statistically significant difference is apparent among the solids at pH 3 with catechol, with AZTD and INFA, showing nearly 2–3× higher %DPb

than USFA and EUFA. This difference highlights the role of ligand-promoted dissolution under acidic conditions, indicating higher preferences for the complexation of catechol with Pb on surface sites in AZTD and INFA than in USFA and EUFA. Theoretical calculations showed that the most stable aqueous phase complex between Pb and catechol is a monodentate complex with a monodeprotonated ligand: $[\text{Pb}(\text{Hcat})(\text{H}_2\text{O})_4]^+_{\text{mono}}$.⁶⁶ This higher preference might be due to a higher density of defect sites containing Pb in the case of the former two solids. In summary, the results in this section clearly show that simulated atmospheric aging conditions, particularly in the pH range 1–7, lead to the dissolution of reactive TE with relatively high amounts compared with the maximum dissolvable fraction from strong acid extraction procedures. The data in this section under dark conditions simulate atmospherically relevant night-time chemistry. Acid-promoted dissolution under dark conditions appears to dominate ligand-promoted dissolution by oxalic acid. On the other hand, the presence of catechol not only changes the optical properties of the dust and fly ash slurries under acidic conditions due to its redox reactivity with Fe, but also lowers the relative amount of dissolvable Fe, Mn, and As. For comparison with data above, the following section presents data on the dissolution of the “fresh” solids studied here in simulated bodily fluids.

3. Soluble Trace Element Content from Simulated Human Exposure Experiments. As stated in the Introduction, several analytical methods are used in the literature to quantify levels of TE extracted in simulated bodily fluids to assess health impacts upon human exposure to atmospheric particles. The efficiency of metal extraction in simulated bodily fluids is generally lower than that in the strong acid extraction procedure described earlier. Here, five methods that cover saliva, gastric, and lung fluids were optimized for measuring the concentrations of Fe, Cu, Mn, As, and Pb (see SI for details).

Figures 5 and S11 show the levels of transition metals extracted from the dust and fly ash samples used here in simulated saliva, lung, and gastric fluids using times that mimic human exposures for 5, 10, and 1 h, respectively. The top panels in Figures 5 and S11 show data normalized to the specific BET surface area of each solid according to eq 2. The bottom panels show the percentages of each element relative to the respective dissolvable element fraction from the strong acid extraction listed in Table S4 according to eq 4:

$$\%DTE = \frac{[TE(aq)](\mu\text{g g}^{-1})}{[TE(aq)]_{\text{acid_extr}}(\mu\text{g g}^{-1})} \cdot 100 \quad (4)$$

These data clearly show that the dissolution of fly ash samples over the simulated exposure times in bodily fluids produced higher Fe, Cu, Mn and Pb than AZTD by at least one order of magnitude. The %DAs in the lower panel of Figure S11 show comparable levels between the AZTD and the fly ash samples, between 5–12%, in the saliva and gastric fluids. In the case of %DPb, the USFA released the highest amount (~13%), followed by EUFA (10%) and INFA (6%) in the 1 h gastric juice, whereas below 1% from the EUFA was dissolved in the Gamble lung fluids compared with none from the INFA and USFA.

As mentioned earlier, residues for all matrices were further digested using microwave digestion. When total concentrations were compared with the summation of the bodily fluid and its respective residue, mass balance was obtained. This means that there was no loss of analyte in the process with the optimization conducted in this study. The pH of saliva and lung fluids is close to neutral (pH of 6.4 and 7.4, respectively) compared to a much more acidic gastric juice (pH of 1.2). Hence, it is not surprising that with an extended extraction and low pH, the majority of TE are found in gastric juice. Still, a greater extraction is seen through the strong acid extraction, with only a fraction being comparable to what is leached by the gastric juice. Bioaccessibility utilizes complex solutions and attempts to determine a larger risk associated with human health. While our optimized procedure here does a great job of showing extractions occurring in every single fluid, it is important to further consider the properties of the samples themselves.

■ ATMOSPHERIC SIGNIFICANCE

Our novel studies showed higher percentages of dissolved TE from atmospheric aging of mineral dust and fly ash particles over 14-d under acidic conditions than in bodily fluids of unreacted particles. These results are significant because they underscore the importance of TE contributions to aerosol multiphase chemistry, health impacts, and ocean biogeochemistry. At the present time, atmospheric aging and human exposure experiments are performed by different research groups and communities that use different materials and do not necessarily interact with each other. Because inhalable atmospheric particles could be freshly emitted or aged, our systematic studies couple atmospheric aging with human exposure experiments using fully characterized reference solid materials, which are representative of atmospheric aerosol particles from natural and combustion sources. The minimum parameters needed as input for environmental and bioaccessibility models are the dissolved concentrations of TE in environmental waters and bodily fluids relative to the maximum dissolvable amounts under strong acid extraction

over relevant time scales and in the presence of WSOC. These models include atmospheric chemistry, global climate, bioaccessibility prediction, health risk assessment, and global oceans. In agreement with earlier published studies cited above, our results show that aging processes over a wide pH range without and with WSOC affect the dissolution of atmospheric particles from natural and combustion sources and increase levels of dissolved TE, particularly under acidic conditions. The dissolved TE in atmospheric waters, from acidic to basic, can catalyze several reactions that change the physicochemical properties of aerosols and droplets with impacts on radiative forcing and cloud and ice nucleation. In addition, inhalation-ingestion of aged and acidic atmospheric particles would contribute potentially more toxic bioaccessible TE Cu, As, and Pb. A likely scenario that highlights this point is a child playing in a local park and being exposed to airborne or deposited dust during playtime. Therefore, it is important to understand and accurately quantify what the exposure risk might be and how impactful or problematic it would be over an extended period. Lastly, the deposition of aged atmospheric particles would likely influence ocean biogeochemistry to a larger extent than freshly emitted ones because they would contribute more dissolved (and very likely more labile) essential micronutrients Fe and Mn and toxicants Cu, As, and Pb to phytoplankton in the SML. The experimental methods and data analyses presented here could serve as benchmarks for future experiments using other lab- and field-collected particles in environmental and bodily fluids. These new experiments need to explore (1) the role of sunlight and ionic strength in atmospheric aging of these particles over the same time frames, (2) the oxidative potential of aged atmospheric particles, and (3) changes to aqueous phase speciation and nanoparticle formation due to changes in WSOC and pH with time to simulate out- and in-cloud processing and ocean water.

■ ASSOCIATED CONTENT

Supporting Information

The Supporting Information is available free of charge at <https://pubs.acs.org/doi/10.1021/acsestair.3c00006>.

Detailed materials and methods, additional figures showing raw data, comparison of extraction method on dissolved metals, percentages of dissolved TE relative to total solid mass, digital images of vials during the atmospheric aging experiments, changes of pH as a function of time during the atmospheric aging experiments, and tables for method optimization, selected dissolved trace element (DTE) content from strong acid extraction experiments in units normalized to mass, the concentration Ca, Mg, and Al from strong acid extraction and atmospheric aging, and list of abbreviations (PDF)

■ AUTHOR INFORMATION

Corresponding Authors

Nausheen W. Sadiq — Department of Chemistry, Mount Royal University, Calgary, AB T3E 6K6, Canada; Phone: (403) 440-8933; Email: nsadiq@mtroyal.ca; Fax: (403)440-8898

Hind A. Al-Abadleh — Department of Chemistry and Biochemistry, Wilfrid Laurier University, Waterloo, ON N2L 3C5, Canada; orcid.org/0000-0002-9425-0646;

Phone: (519)884-0710; Email: halabadleh@wlu.ca;
Fax: (519)746-0677

Authors

Catharina Venter – Department of Chemistry, Mount Royal University, Calgary, AB T3E 6K6, Canada

Wisam Mohammed – Department of Chemistry and Biochemistry, Wilfrid Laurier University, Waterloo, ON N2L 3C5, Canada

Yara Khalaf – Department of Chemistry and Biochemistry, Wilfrid Laurier University, Waterloo, ON N2L 3C5, Canada

Complete contact information is available at:
<https://pubs.acs.org/10.1021/acsestair.3c00006>

Notes

The authors declare no competing financial interest.

ACKNOWLEDGMENTS

N.W.S. acknowledges funding and support from Mount Royal University. H.A.A. acknowledges partial funding from Laurier, NSERC, and the Canadian Foundation for Innovation. The authors thank Professor Juan Navea from Skidmore College for sharing with us the coal fly ash samples from his lab. The authors would like to thank Dr. Carmen Andrei in the Canadian Centre for Electron Microscopy at McMaster University for collecting the HAADF-STEM images, and Victoria Jarvis in the MAX Diffraction Facility at McMaster University for collecting the XRD spectra.

REFERENCES

- (1) Choobari, O. A.; Zawar-Reza, P.; Sturman, A. The global distribution of mineral dust and its impacts on the climate system: A review. *Atmos. Res.* **2014**, *138*, 152–165.
- (2) Schepanski, K. Transport of mineral dust and its impact on climate. *Geosciences* **2018**, *8*, 151.
- (3) Adebisi, A. A.; Huang, Y.; Samsat, B. H.; Kok, J. F. Observations suggest that north african dust absorbs less solar radiation than models estimate. *Commun. Earth Environ.* **2023**, *4*, 168.
- (4) Barkley, A. E.; Olson, N. E.; Prospero, J. M.; Gatineau, A.; Panachou, K.; Maynard, N. G.; Blackwelder, P.; China, S.; Ault, A. P.; Gaston, C. J. Atmospheric transport of North African dust-bearing supermicron freshwater diatoms to South America: Implications for iron transport to the equatorial north atlantic ocean. *Geophys. Res. Lett.* **2021**, *48*, No. e2020GL090476.
- (5) Ryder, C. L.; Highwood, E. J.; Walsler, A.; Seibert, P.; Philipp, A.; Weinzierl, B. Coarse and giant particles are ubiquitous in Saharan dust export regions and are radiatively significant over the Sahara. *Atmos. Chem. Phys.* **2019**, *19*, 15353–15376.
- (6) Ryder, C. L.; Marengo, F.; Brooke, J. K.; Estelles, V.; Cotton, R.; Formenti, P.; McQuaid, J. B.; Price, H. C.; Liu, D.; Ausset, P.; et al. Coarse-mode mineral dust size distributions, composition and optical properties from AER-D aircraft measurements over the tropical eastern atlantic. *Atmos. Chem. Phys.* **2018**, *18*, 17225–17257.
- (7) Boucher, O.; Randall, D.; Artaxo, P.; Bretherton, C.; Feingold, G.; Forster, F.; Kerminen, V.-M.; Kondo, Y.; Liao, H.; Lohmann, U.; Rasch, P.; Satheesh, S. K.; Sherwood, S.; Stevens, B.; Zhang, X. Y. Clouds and aerosols. In *Climate change 2013: The physical science basis. Contribution of working group I to the fifth assessment report of the intergovernmental panel on climate change*; Stocker, T. F., Qin, D., Plattner, G.-K., Tignor, M., Allen, S. K., Boschung, J., Nauels, A., Xia, Y., Bex, V., Midgley, P. M., Eds.; Cambridge University Press: Cambridge, United Kingdom and New York, NY, U.S.A., 2013; pp 571–657.
- (8) Textor, C.; Schulz, M.; Guibert, S.; Kinne, S.; Balkanski, Y.; Bauer, S.; Bernsten, T.; Berglen, T.; Boucher, O.; Chin, M.; et al. Analysis and quantification of the diversities of aerosol life cycles within AEROCOM. *Atmos. Chem. Phys.* **2006**, *6*, 1777–1813.
- (9) Griffin, D. W.; Kellogg, C. A.; Shinn, E. A. Dust in the wind: Long range transport of dust in the atmosphere and its implications for global public and ecosystem health. *Global Change Human Health* **2001**, *2*, 20–33.
- (10) Philip, S.; Martin, R. V.; Snider, G.; Weagle, C. L.; van Donkelaar, A.; Brauer, M.; Henze, D. K.; Klimont, Z.; Venkataraman, C.; Guttikunda, S. K.; Zhang, Q. Anthropogenic fugitive, combustion and industrial dust is a significant, underrepresented fine particulate matter source in global atmospheric models. *Environ. Res. Lett.* **2017**, *12*, 044018.
- (11) Junkermann, W.; Hacker, J. Unprecedented levels of ultrafine particles, major sources, and the hydrological cycle. *Sci. Rep.* **2022**, *12*, 7410.
- (12) White, S. C.; Case, E. D. Characterization of fly ash from coal-fired power plants. *J. Mater. Sci.* **1990**, *25*, 5215–5219.
- (13) Zyrkowski, M.; Neto, R. C.; Santos, L. F.; Witkowski, K. Characterization of fly-ash cenospheres from coal-fired power plant unit. *Fuel* **2016**, *174*, 49–53.
- (14) Demirbas, A. Heavy metal contents of fly ashes from selected biomass samples. *Energy Sources* **2005**, *27*, 1269–1276.
- (15) Li, R.; Zhang, H.; Wang, F.; Ren, Y.; Jia, S.; Jiang, B.; Jia, X.; Tang, Y.; Tang, M. Abundance and fractional solubility of phosphorus and trace metals in combustion ash and desert dust: Implications for bioavailability and reactivity. *Sci. Total Environ.* **2022**, *816*, No. 151495.
- (16) Chen, H.; Laskin, A.; Baltrusaitis, J.; Gorski, C. A.; Scherer, M. M.; Grassian, V. H. Coal fly ash as a source of iron in atmospheric dust. *Environ. Sci. Technol.* **2012**, *46*, 2112–2120.
- (17) Ghio, A. J.; Carraway, M. S.; Madden, M. C. Composition of air pollution particles and oxidative stress in cells, tissues, and living systems. *J. Toxicol. Environ. Health B: Crit. Rev.* **2012**, *15*, 1–21.
- (18) Rauch, J. N.; Pacyna, J. M. Earth's global Ag, Al, Cr, Cu, Fe, Ni, Pb and Zn cycles. *Global Biogeochem. Cyc.* **2009**, *23*, No. GB2001.
- (19) Tilgner, A.; Schaefer, T.; Alexander, B.; Barth, M. C.; Collett, J. L., Jr.; Fahey, K. M.; Nenes, A.; Pye, H. O. T.; Herrmann, H.; McNeill, V. F. Acidity and the multiphase chemistry of atmospheric aqueous particles and clouds. *Atmos. Chem. Phys.* **2021**, *21*, 13483–13536.
- (20) Shi, Z. B.; Krom, M. D.; Jickells, T. D.; Bonneville, S.; Carslaw, K. S.; Mihalopoulos, N.; Baker, A. R.; Benning, L. G. Impacts on iron solubility in the mineral dust by processes in the source region and the atmosphere: A review. *Aeolian Res.* **2012**, *5*, 21–42.
- (21) Shi, Z.; Krom, M. D.; Bonneville, S.; Benning, L. G. Atmospheric processing outside clouds increases soluble iron in mineral dust. *Environ. Sci. Technol.* **2015**, *49*, 1472–1477.
- (22) Shi, Z.; Krom, M. D.; Bonneville, S.; Baker, A. R.; Jickells, T. D.; Benning, L. G. Formation of iron nanoparticles and increase in iron reactivity in mineral dust during simulated cloud processing. *Environ. Sci. Technol.* **2009**, *43*, 6592–6596.
- (23) Al-Abadleh, H. A.; Nizkorodov, S. A. Open questions on transition metals driving secondary thermal processes in atmospheric aerosols. *Commun. Chem.* **2021**, *4*, 1–4.
- (24) Deguillaume, L.; Leriche, M.; Desboeufs, K.; Mailhot, G.; George, C.; Chaumerliac, N. Transition metals in atmospheric liquid phases: Sources, reactivity, and sensitive parameters. *Chem. Rev.* **2005**, *105*, 3388–3431.
- (25) Al-Abadleh, H. A. Aging of atmospheric aerosols and the role of iron in catalyzing brown carbon formation. *Environ. Sci.: Atmos.* **2021**, *1*, 297–345.
- (26) Al-Abadleh, H. A.; Kubicki, J. D.; Meskhidze, N. A perspective on iron (Fe) in the atmosphere: Air quality, climate, and the ocean. *Environ. Sci.: Processes Impacts* **2023**, *25*, 151–164.
- (27) Chen, L.; Peng, C.; Gu, W.; Fu, H.; Jian, X.; Zhang, H.; Zhang, G.; Zhu, J.; Wang, X.; Tang, M. On mineral dust aerosol hygroscopicity. *Atmos. Chem. Phys.* **2020**, *20*, 13611–13626.
- (28) Pye, H. O. T.; Nenes, A.; Alexander, B.; Ault, A. P.; Barth, M. C.; Clegg, S. L.; Collett, J. L., Jr.; Fahey, K. M.; Hennigan, C. J.

- Herrmann, H.; Kanakidou, M.; Kelly, J. T.; Ku, I.-T.; McNeill, V. F.; Riemer, N.; Schaefer, T.; Shi, G.; Tilgner, A.; Walker, J. T.; Wang, T.; Weber, R.; Xing, J.; Zaveri, R. A.; Zuend, A. The acidity of atmospheric particles and clouds. *Atmos. Chem. Phys.* **2020**, *20*, 4809–4888.
- (29) Al-Abadleh, H. A. *Atmospheric Aerosol Chemistry: State of the Science*; De Gruyter: Berlin/Boston, 2022.
- (30) Denjean, C.; Formenti, P.; Desboeufs, K.; Chevaillier, S.; Triquet, S.; Maille, M.; Cazaunau, M.; Laurent, B.; Mayol-Bracero, O. L.; Vallejo, P.; Quinones, M.; Gutierrez-Molina, I. E.; Cassola, F.; Prati, P.; Andrews, E.; Ogren, J. Size distribution and optical properties of African mineral dust after intercontinental transport. *J. Geophys. Res.-Atmos.* **2016**, *121*, 7117–7138.
- (31) China, S.; Mazzoleni, C. Preface: Morphology and internal mixing of atmospheric particles. *Atmosphere* **2018**, *9*, 249.
- (32) Riemer, N.; Ault, A. P.; West, M.; Craig, R. L.; Curtis, J. H. Aerosol mixing state: Measurements, modeling, and impacts. *Rev. Geophys.* **2019**, *57*, 187–249.
- (33) Fang, T.; Guo, H.; Zeng, L.; Verma, V.; Nenes, A.; Weber, R. J. Highly acidic ambient particles, soluble metals, and oxidative potential: A link between sulfate and aerosol toxicity. *Environ. Sci. Technol.* **2017**, *51*, 2611–2620.
- (34) Abou Chakra, O. R.; Joyeux, M.; Nerriere, E.; Strub, M. P.; Zmirou-Navier, D. Genotoxicity of organic extracts of urban airborne particulate matter: An assessment within a personal exposure study. *Chemosphere* **2007**, *66*, 1375–1381.
- (35) Hamilton, D. S.; Perron, M. M. G.; Bond, T. C.; Bowie, A. R.; Buchholz, R. R.; Guieu, C.; Ito, A.; Maenhaut, W.; Myriokefalitakis, S.; Olgun, N.; Rathod, S. D.; Schepanski, K.; Tagliabue, A.; Wagner, R.; Mahowald, N. M. Earth, wind, fire, and pollution: Aerosol nutrient sources and impacts on ocean biogeochemistry. *Annu. Rev. Mar. Sci.* **2022**, *14*, 303–330.
- (36) Mahowald, N. M.; Hamilton, D. S.; Mackey, K. R. M.; Moore, J. K.; Baker, A. R.; Scanza, R. A.; Zhang, Y. Aerosol trace metal leaching and impacts on marine microorganisms. *Nat. Commun.* **2018**, *9*, 2614.
- (37) Paytan, A.; Mackey, K. R. M.; Chen, Y.; Lima, I. D.; Doney, S. C.; Mahowald, N.; Labiosa, R.; Post, A. F. Toxicity of atmospheric aerosols on marine phytoplankton. *Proc. Natl. Acad. Sci. U.S.A.* **2009**, *106*, 4601–4605.
- (38) Ohlwein, S.; Kappeler, R.; Joss, M. K.; Kunzli, N.; Hoffmann, B. Health effects of ultrafine particles: A systematic literature review update of epidemiological evidence. *Int. J. Public Health* **2019**, *64*, 547–559.
- (39) Karotki, D. G.; Bekö, G.; Clausen, G.; Madsen, A. M.; Andersen, Z. J.; Massling, A.; Ketzler, M.; Ellermann, T.; Lund, R.; Sigsgaard, T.; Möller, P.; Loft, S. Cardiovascular and lung function in relation to outdoor and indoor exposure to fine and ultrafine particulate matter in middleaged subjects. *Environ. Int.* **2014**, *73*, 372–381.
- (40) Park, M.; Joo, H. S.; Lee, K.; Jang, M.; Kim, S. D.; Kim, I.; Borlaza, L. J. S.; Lim, H.; Shin, H.; Chung, K. H.; Choi, Y.-H.; Park, S. G.; Bae, M.-S.; Lee, J.; Song, H.; Park, K. Differential toxicities of fine particulate matters from various sources. *Sci. Rep.* **2018**, *8*, 17007.
- (41) Grigoratos, T.; Martini, G. Brake wear particle emissions: A review. *Environ. Sci. Pollut. Res. Int.* **2015**, *22*, 2491–2504.
- (42) Shiraiwa, M.; Ueda, K.; Pozzer, A.; Lammel, G.; Kampf, C. J.; Fushimi, A.; Enami, S.; Arangio, A. M.; Frohlich-Nowoisky, J.; Fujitani, Y.; Furuyama, A.; Lakey, P. S. J.; Lelieveld, J.; Lucas, K.; Morino, Y.; Poschl, U.; Takahama, S.; Takami, A.; Tong, H.; Weber, B.; Yoshino, A.; Sato, K. Aerosols health effects from molecular to global scales. *Environ. Sci. Technol.* **2017**, *51*, 13545–13567.
- (43) Weichenthal, S. A.; Pollitt, K. G.; Villeneuve, P. J. PM_{2.5}, oxidant defence and cardiorespiratory health: A review. *Environ. Health* **2013**, *12*, 1–8.
- (44) Shi, W.; Li, T.; Zhang, Y.; Sun, Q.; Chen, C.; Wang, J.; Fang, J.; Zhao, F.; Du, P.; Shi, X. Depression and anxiety associated with exposure to fine particulate matter constituents: A cross-sectional study in North China. *Environ. Sci. Technol.* **2020**, *54*, 16006–16016.
- (45) Landrigan, P. J.; Fuller, R.; Acosta, N. J. R.; Adeyi, O.; Arnold, R.; Basu, N.; Baldé, A. B.; Bertollini, R.; Bose-O'Reilly, S.; Boufford, J. I.; Breyse, P. N.; Chiles, T.; Mahidol, C.; Coll-Seck, A. M.; Cropper, M. L.; Fobil, J.; et al. The lancet commission on pollution and health. *Lancet* **2018**, *391*, 462–512.
- (46) Kastury, F.; Smith, E.; Karna, R. R.; Scheckel, K. G.; Juhasz, A. L. An inhalation-ingestion bioaccessibility assay (IIBA) for the assessment of exposure to metal(loid)s in PM₁₀. *Sci. Total Environ.* **2018**, *631–632*, 92–104.
- (47) Tacu, I.; Kokalari, I.; Abollino, O.; Albrecht, C.; Malandrino, M.; Ferretti, A. M.; Schins, R. P. F.; Fenoglio, I. Mechanistic insights into the role of iron, copper, and carbonaceous component on the oxidative potential of ultrafine particulate matter. *Chem. Res. Toxicol.* **2021**, *34*, 767–779.
- (48) Fernandez-García, E.; Carvajal-Lerida, I.; Perez-Galvez, A. In vitro bioaccessibility assessment as a prediction tool of nutritional efficiency. *Nutr. Res.* **2009**, *29*, 751–760.
- (49) Wurl, O.; Ekau, W.; Landing, W. M.; Zappa, C. J. Sea surface microlayer in a changing ocean – a perspective. *Elem. Sci. Anth.* **2017**, *5*, 1–11.
- (50) Sparks, D. L.; Singh, B.; Siebecker, M. G. *Environmental Soil Chemistry*, 3rd ed.; Academic Press, Elsevier: U.S.A. and U.K., 2023.
- (51) Scheffler, G. L.; Sadiq, N. W.; Pozebon, D.; Beauchemin, D. Risk assessment of trace elements in airborne particulate matter deposited on air filters using solid sampling ETV-ICPOES to measure total concentrations and leaching with simulated saliva, gastric juice and lung fluid to estimate bio-accessibility. *J. Anal. Atom. Spectrom.* **2018**, *33*, 1486–1492.
- (52) Kim, D.; Xiao, Y.; Karchere-Sun, R.; Richmond, E.; Ricker, H. M.; Leonardi, A.; Navea, J. G. Atmospheric processing of anthropogenic combustion particles: Effects of acid media and solar flux on the iron mobility from fly ash. *ACS Earth Space Chem.* **2020**, *4*, 750–761.
- (53) Borgatta, J.; Paskavitz, A.; Kim, D.; Navea, J. G. Comparative evaluation of iron leach from fly ash from different source regions under atmospherically relevant conditions. *Environ. Chem.* **2016**, *13*, 902–912.
- (54) Link, N.; Removski, N.; Yun, J.; Fleming, L.; Nizkorodov, S. A.; Bertram, A. K.; Al-Abadleh, H. A. Dust-catalyzed oxidative polymerization of catechol under acidic conditions and its impacts on ice nucleation efficiency and optical properties. *ACS Earth Space Chem.* **2020**, *4*, 1127–1139.
- (55) Innes, E.; Yiu, H. P. H.; McLean, P.; Brown, W.; Boyles, M. Simulated biological fluids – a systematic review of their biological relevance and use in relation to inhalation toxicology of particles and fibres. *Crit. Rev. Toxicol.* **2021**, *51*, 217–248.
- (56) Sadiq, N. W.; Beauchemin, D. Simultaneous speciation analysis of arsenic, chromium, and selenium in the bioaccessible fraction for realistic risk assessment of food safety. *Anal. Chem.* **2017**, *89*, 13299–13304.
- (57) EPA. Method 6020b (SW-846): Inductively coupled plasma - mass spectrometry. <https://www.epa.gov/esam/epa-method-6020b-sw-846-inductively-coupled-plasma-mass-spectrometry> (accessed 2023–07–28).
- (58) Method 200.2, revision 2.8: Sample preparation procedure for spectrochemical determination of total recoverable elements. https://19january2017snapshot.epa.gov/sites/production/files/2015-08/documents/method_200-2_rev_2-8_1994.pdf (accessed 2023–07–28).
- (59) Chen, H.; Grassian, V. H. Iron dissolution of dust source materials during simulated acidic processing: The effect of sulfuric, acetic, and oxalic acids. *Environ. Sci. Technol.* **2013**, *47*, 10312–10321.
- (60) Rubasinghege, G.; Lentz, R. W.; Scherer, M. M.; Grassian, V. H. Simulated atmospheric processing of iron oxyhydroxide minerals at low pH: Roles of particle size and acid anion in iron dissolution. *Proc. Natl. Acad. Sci. U.S.A.* **2010**, *107*, 6628–6633.
- (61) Banuelos, J. L.; Borguet, E.; Brown, G. E., Jr.; Cygan, R. T.; DeYoreo, J.; Dove, P. M.; Gageot, M.-P.; Geiger, F. M.; Gibbs, J. M.; Grassian, V. H.; Ilgen, A. G.; Jun, Y.-S.; Kabengi, N.; Katz, L.; Kubicki,

J. D.; Lutzenkirchen, J.; Putnis, C. V.; Remsing, R. C.; Rosso, K. M.; Rother, G.; Sulpizi, M.; Villalobos, M.; Zhang, H. Oxide– and silicate–water interfaces and their roles in technology and the environment. *Chem. Rev.* **2023**, *123*, 6413–6544.

(62) Maier, G. P.; Bernt, C. M.; Butler, A. Catechol oxidation: Considerations in the design of wet adhesive materials. *Biomater. Sci.* **2018**, *6*, 332–339.

(63) Mentasti, E.; Pelizzetti, E. Reactions between iron(III) and catechol (o-dihydroxybenzene). Part I. Equilibria and kinetics of complex formation in aqueous acid solution. *J. Chem. Soc., Dalton Trans.* **1973**, *1*, 2605–2608.

(64) Situm, A.; Rahman, M. A.; Goldberg, S.; Al-Abadleh, H. A. Spectral characterization and surface complexation modeling of organics on hematite nanoparticles: Role of electrolytes in the binding mechanism. *Environ. Sci. Nano* **2016**, *3*, 910–926.

(65) Paris, R.; Desboeufs, K. V. Effect of atmospheric organic complexation on iron-bearing dust solubility. *Atmos. Chem. Phys.* **2013**, *13*, 4895–4905.

(66) Lapouge, C.; Cornard, J. P. Theoretical study of the Pb(II)–catechol system in dilute aqueous solution: Complex structure and metal coordination sphere determination. *J. Mol. Struct.* **2010**, *969*, 88–96.